

# A Film Boiling Study of Ethanol Pyrolysis

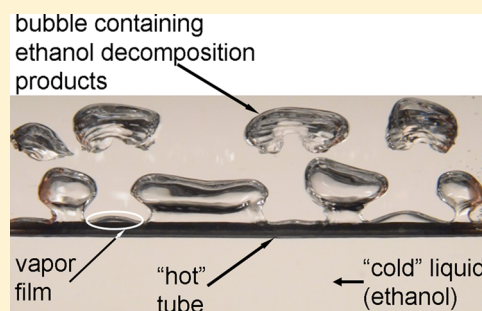
C. Thomas Avedisian,<sup>\*,†,‡</sup> Wei-Chih Kuo,<sup>†,□</sup> Wing Tsang,<sup>‡</sup> and Adam Lowery<sup>†,○</sup>

<sup>†</sup>Sibley School of Mechanical and Aerospace Engineering, Cornell University, Ithaca, New York 14853-7501, United States

<sup>‡</sup>Physical and Chemical Properties Division, National Institute of Standards and Technology, Gaithersburg, Maryland 20899, United States

## S Supporting Information

**ABSTRACT:** This paper reports a study of ethanol pyrolysis ( $C_2H_5OH$ , EtOH) by film boiling at temperatures ranging from 600 to 1500 K. The reactor space is created in a self-assembled manner by first bringing EtOH to a boil on the surface of a horizontal tube submerged in a pool of EtOH and then increasing the power to the tube in steps to force transitioning the boiling regimes through nucleate boiling, the critical heat flux state, and finally film boiling. EtOH pyrolysis is found to yield hydrogen in the highest concentration followed by ethylene ( $C_2H_4$ ), methane ( $CH_4$ ), and carbon monoxide (CO) in approximately equal proportions. Ethane ( $C_2H_6$ ) and carbon dioxide (CO) concentrations were several orders of magnitude lower. The abundance of hydrogen was conjectured to be due to the absence of chemical inhibitors in the system. Reactions to explain formation of the product gases are suggested based on the chain nature of EtOH decomposition. Liquid sampling showed the presence of refluxed water along with acetaldehyde ( $CH_3CHO$ ) and trace quantities of formaldehyde ( $CH_2O$ ) and ethyl acetate ( $CH_3COOC_2H_5$ ). Evidence of heterogeneous surface reactions is postulated for tube temperatures below about 1000 K. The results are consistent with more conventional reactor designs, which establishes the potential for film boiling to serve as a simple and useful chemical processing technology.



## 1. INTRODUCTION

Ethanol ( $C_2H_5OH$ , EtOH, normal boiling point 352 K) is widely used as a biofuel additive in commercial gasoline blends (e.g., E10). It has attracted much attention for this application as well as to understand its fundamental oxidation kinetics.<sup>1–17</sup> Equally important is the thermal decomposition of EtOH because pyrolysis reactions are embedded in oxidation kinetics. Experimental designs used in EtOH decomposition studies have included shock tubes, various reactor designs (e.g., tubular flow reactors and jet-stirred and packed bed reactors), and laminar premixed flame configurations. The temperature ranges covered regimes influenced to an extent by heterogeneous (surface) reactions at low temperatures and homogeneous (bulk) decomposition at high temperatures with theoretical predictions reported up to 2000 K.<sup>1,4–6</sup>

The experimental configurations provide a thermal environment for decomposition characterized by a well-defined temperature in the reaction zone. They are rather stationary installations well suited for laboratory scale studies. A reactor design that is conceptually mobile so the reactor could be brought to the reactant, that does not need pumps to transport fluid through the reaction zone, or hardware to prevaporize chemicals that are liquid in the standard atmosphere, and is easily fabricated while being capable of providing fundamental information about reaction chemistry would be a useful alternative. This paper describes such a reactor and uses it to study decomposition of EtOH.

EtOH decomposes by a well-known process as noted above and, as such, there was no expectation of significant differences

with the literature. On the other hand, identifying product species and comparing with literature values provides a means to assess performance under film boiling conditions. In this way, and by showing a consistency with results using other reactor designs, film boiling as a chemical processing technology could then be applied to new and complex systems with confidence in the results.

The reactor design is based on the film boiling regime of multiphase heat transport. In this boiling mode, the surface on which film boiling is established is covered with a thin vapor film that provides a reactor space and thermal conditions which promote decomposition of the gases flowing within it. Figure 1a schematically illustrates this configuration for a horizontal tube (other heater configurations for supporting film boiling can be envisioned for present purposes as well (e.g., flat plate)). Figure 1b shows the vapor flow paths involved with the design.

Film boiling has several features useful for studying thermal decomposition. Perhaps most importantly is its potential to create surface temperatures sufficient to promote decomposition. This potential is derived from the insulating effect of the vapor film that covers the surface. Moreover, unlike any other chemical processing technology, a reactor based on film boiling does not need to be fabricated in the conventional sense. Instead, it essentially builds itself, or is self-assembled, by

**Received:** February 19, 2018

**Revised:** April 26, 2018

**Accepted:** May 4, 2018

**Published:** May 4, 2018

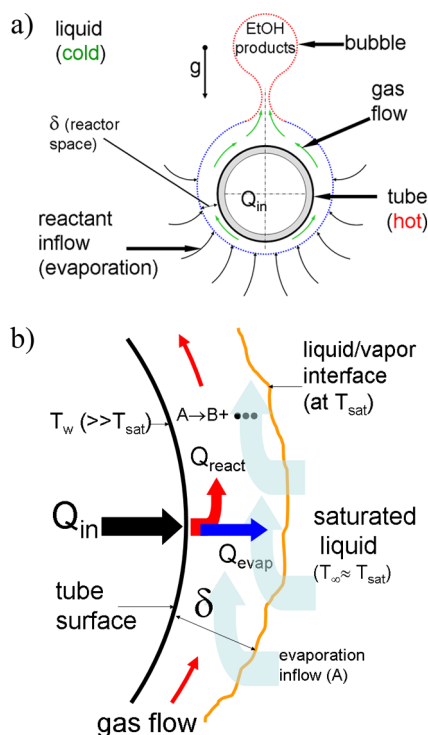


**Figure 1.** (a) Schematic of film boiling on a horizontal tube (section a-a of Figure 3c); (b) schematic of vapor flow and reactive paths for endothermic decomposition of A (EtOH) in film of thickness  $\delta$ .

the natural transition of the multiphase heat transfer states associated with progressive heating of the tube (Figure 1) from single phase convection to nucleate boiling and finally to the film boiling configuration depicted in Figure 1. A single process variable (surface temperature) controls development of the reactor space and the thermal environment for decomposition, and when operated in a buoyancy field as in the present study no pumps are required to transport gases inside the film.

At sufficiently high temperatures in the vapor film, the gases will decompose at appreciable rates forming products in sufficiently high concentration that they can be identified and their concentrations measured. The gases collect in the bubbles that form and pinch off the tube and then percolate through the liquid pool. Bubble transport is dictated by the buoyancy forces acting on the bubbles. The bubble contents are released when they reach the free liquid surface of the pool. They are then analyzed as the gases pass out of the system and through flow meters and gas detection equipment.

An oversimplification of EtOH decomposition is by a unimolecular route that forms only  $\text{H}_2\text{O}$  and  $\text{C}_2\text{H}_4$ :<sup>1–3,18–21</sup>



(the rate constant is expressed by the Arrhenius form,

$K_1 = A_1 \exp\left(-\frac{E_1}{R_g T}\right)$  where  $R_g$  is the gas constant,  $E_1$  is the activation energy, and  $A_1$  is the frequency factor for the reaction (which may depend weakly on temperature). In reality, EtOH decomposition can involve multiple chain-branching reactions to produce other stable species, especially in the absence of chemical inhibitors.<sup>2,6,20–23</sup> In this event, hydrogen will be produced, which is of particular interest as an energy source.<sup>24,25</sup>

The next section discusses the experimental arrangement and procedures. Section 3.1 describes the operational domain for EtOH film boiling, and the Supporting Information includes a video showing development of the reactor volume. A discussion of results is then presented in Section 3.2.

## 2. EXPERIMENT

The results reported here were obtained using the experimental design described in ref 26 where more details can be found. A brief description of the apparatus and procedure is presented in this section. All of the experimental results were obtained under atmospheric pressure.

The apparatus consists of a 4.4 L glass chamber with metal flanges at the ends and feed-thru fittings partially filled with 3.5 L of EtOH. A horizontal tube, attached at the ends by copper clamps with electrical busses for supplying power to the tube, is positioned in the chamber and submerged in the EtOH pool. The tube is electrically heated in steps (see below) to transition EtOH to the film boiling regime. The gases exit the chamber and pass through condensers in a configuration that allows condensable products to reflux to the pool.

Because of refluxing, the initially pure EtOH pool is transformed into a miscible mixture of condensable products with EtOH during operation. The liquid is sampled periodically and analyzed offline using GC/MS to identify the condensable products and their relative amounts. Table 1 shows the liquid

**Table 1. Mole Fraction of Condensable Products in the 3.5 L Liquid Pool after 4 Hours of Continuous Operation at a Tube Temperature of Approximately 1206 K**

chemical	formula	$T_b$ (K)	mole fraction	mole fraction relative to EtOH
ethanol	$\text{C}_2\text{H}_5\text{OH}$	351	0.9498	1.0
acetaldehyde	$\text{CH}_3\text{CHO}$	293	0.0375	0.03948
water	$\text{H}_2\text{O}$	373	0.0099	0.01042
formaldehyde	$\text{CH}_2\text{O}$	254	0.0013	0.00014
1,1-diethoxyethane	$\text{CH}_3\text{CH}(\text{OC}_2\text{H}_5)_2$	376	0.0011	0.00012
ethyl acetate	$\text{CH}_3\text{COOC}_2\text{H}_5$	350	0.0005	0.00005

pool composition at a tube temperature of 1206 K. The condensable in highest relative concentration is acetaldehyde, whose decomposition is part of the reaction network discussed in Section 3.2 to explain the product gases formed.

The condensables can be preferentially vaporized at the interface between the vapor film and liquid and enter the reactor volume defined by the vapor film surrounding the tube. Within the film, they decompose while flowing in the film under the action of buoyancy (cf, Figure 1). Noncondensable gases pass out of the system with a small flow passing through a gas chromatograph to identify the noncondensable product gases and their concentrations. The liquid level in the chamber is maintained throughout an experiment by slowly feeding fresh EtOH into the bottom of the chamber as needed. It is noted that the alternative to this flow configuration is to prevent refluxing, in which case the EtOH would remain pure throughout operation.

An Inconel 600 tube is used as a substrate to support film boiling, which was 2.38 mm OD, 1.88 mm ID, and with an active boiling region of 60 mm. A ceramic tube insert provides structural support to minimize sagging of the tube at the upper levels of temperature especially near its melting point. Two

thermocouples are positioned within the ceramic insert to monitor the tube temperature during power increments. Prior to an experiment, the tube was polished. A new tube was used for each repetition.

The data acquisition system consists of two flow meters in parallel (with different ranges of sensitivity), a programmable digital power supply, a personal computer (PC), and a gas chromatograph (Gow-Mac Instruments Series 600-TCD gas chromatograph). A LabVIEW program controls power increments to the tube (through an Agilent 6681A digital power supply) and stores temperature, voltages, and currents in the PC. An array of immersion heaters is mounted in the liquid pool to control liquid temperature. EtOH is kept to within a few degrees of its saturation temperature throughout operation.

Film boiling is established in a procedure that involves first immersing the tube into the EtOH pool and then increasing power to the tube in 0.1 V increments to transition the heat transfer modes from single phase convection, to nucleate boiling, the critical heat flux (CHF) point, and ultimately film boiling. After each voltage increment, the system is allowed to reach steady state (about 5 min). During the transition from one steady state condition to the next, the 0.1 V increment typically corresponds to heating rates between 0.1 and 0.4 K/s.

A video showing the transition from nucleate to film boiling of EtOH is included in the [Supporting Information](#). In the video, film boiling is shown to be established at the left side of the tube. The transition front from nucleate to film boiling moves to the right. The copper power clamps are visible at each end. The video was operated at 24 frames per second. The initiation of film boiling occurs approximately 8 s after the video is started. The transition front did not occur at the same location (left, right, or near center) for all tubes used in the experiments.

Attempts to raise the heat flux above the CHF initiates development of a vapor film and film boiling. Once in film boiling, the tube temperature is varied by incrementally by increasing power to it. At each power setting, the bulk liquid and tube temperatures, the electrical current through the tube, exhaust gas flow rates, and gas compositions are all recorded electronically. The upper temperature limit of the results reported is about 1500 K, at which level the tube would buckle (the melting point of Inconel is 1686 K), and the experiment then stopped.

An important consideration in identifying an appropriate temperature for decomposition concerns the large temperature variation across the vapor film (thickness  $\delta$  in [Figure 1](#)). A simple model was developed<sup>26</sup> to specify a suitable reaction temperature. It is based on considering that most of the conversion in the vapor film will occur within a small layer near the tube surface because of the strong dependence of the conversion rate on temperature for Arrhenius kinetics. It was judged that the tube temperature  $T_w$  can characterize the thermal environment for the reaction in some cases, especially at lower temperatures. When presenting the experimental data in the next section,  $T_w$  is used as the representative temperature with the above consideration in mind.

### 3. RESULTS AND DISCUSSION

**3.1. EtOH Boiling Curve.** The boiling curve of a liquid<sup>27</sup> delineates the operational boundaries of heat flux and temperature for film boiling. At low heat fluxes ( $q_2''$  and temperature ( $T_2$ )), the vapor film begins to destabilize because the temperature is too low to maintain separation of the vapor

film from the surface, and the vapor film begins to break down as liquid/solid contact occurs.

As shown in [Figure 2](#), at low temperatures ( $<T_1$ ), EtOH is in nucleate boiling where the temperature is low and decom-

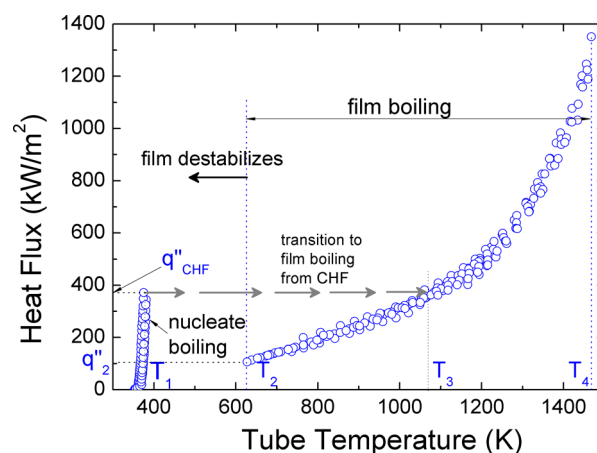


**Figure 2.** Boiling curve of EtOH showing the CHF and minimum film boiling temperatures. On transition from CHF to film boiling, the tube temperature jumps from  $T_1$  to  $T_3$  (i.e., across the transition front shown in the video of film boiling of EtOH provided in the [Supporting Information](#)).  $T_4$  is the upper limit before the tube would be damaged, while at  $T_2$ , the film is destabilized, and the reactor space disappears.

position is unlikely to occur at an appreciable rate because the minimum temperature for unimolecular decomposition of EtOH appears to be over 700 K.<sup>6</sup>

Once CHF is reached, the tube temperature jumps to  $T_3$ , and the tube then becomes covered with vapor. Upon lowering the heat flux in the film boiling regime the film will destabilize at temperature,  $T_2$ , because of insufficient energy to the liquid to maintain the bubble population: the vapor film collapses and the reactor space then disappears. Within the range  $T_2$  to  $T_4$ , the vapor film is maintained by heat transfer to the fluid, and decomposition is possible.

Few elements of the boiling curve are predictable from first principles. A high degree of empiricism is required because of the dependence of the need to know the surface topology such as surface imperfections and their distribution and morphology (size and shape), which are unique to surface finish and not generally predictable from first principles. In this case various constants are introduced into the formulations that are found to best match measurements. An exception is the CHF.

It is generally accepted that the coalescence of bubbles near the CHF is responsible for choking off the return flow of liquid to the surface as the bubbles try to escape, which leads to the temperature excursion  $T_1$  to  $T_3$  (i.e., across the transition front shown in the companion video of the paper in the [Supporting Information](#)). The measured CHF shown in [Figure 2](#) is 372 kW/m<sup>2</sup> at 375 K. The predicted value, accounting for the effect of the tube size<sup>27</sup> and using EtOH properties at saturation, is 451 kW/m<sup>2</sup>. The 18% difference is within the range of applicability of the formulations.

The transition from nucleate to film boiling ( $T_1$  to  $T_3$  in [Figure 2](#)) is represented by the photographs in [Figure 3](#). [Figure 3a](#) shows the bubble morphology in nucleate boiling. A plethora of bubbles line the tube surface where they form at distinct nucleation sites and do not coalesce. As the heat flux is increased ([Figure 3b](#)), the bubble population increases, and the

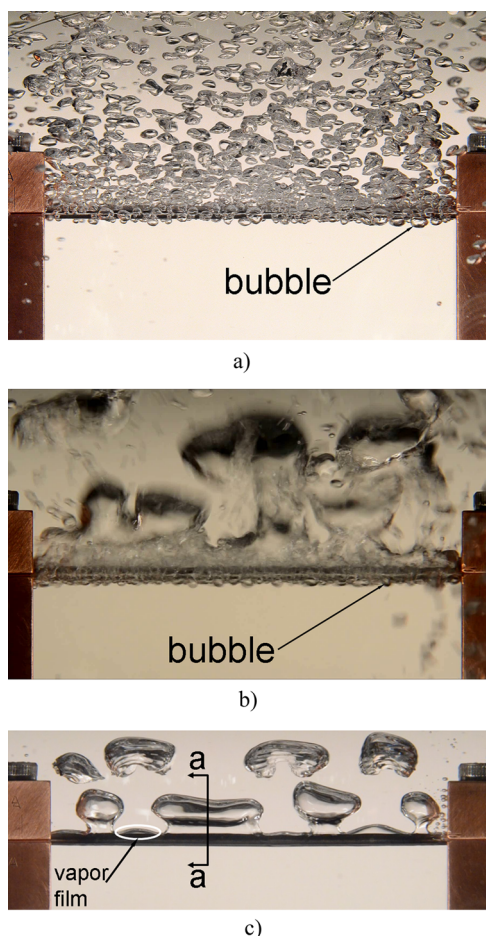


**Figure 3.** Selected photographs showing boiling configurations of saturated ethanol. (a) Nucleate boiling,  $T_w = 370$  K; (b) transition region; (c) film boiling at  $T_w = 638$  K. Bubbles in panel c contain decomposition products. Vapor film in which decomposition occurs is indicated. A schematic of section a-a in panel c is given in Figure 1a. Tube diameter is 2.38 mm.

bubbles begin to coalesce. At high input fluxes to the tube, the departing bubbles completely coalesce and form a vapor layer around the tube (Figure 3c). The reactor space is within this vapor layer, and the bubbles shown in Figure 3c will ostensibly contain the reaction products.

The bubble morphology shown in Figure 3c is consistent with detailed simulations of film boiling which include three-dimensional effects.<sup>28–31</sup> The bubble configuration is similar to predicted shapes though the simulations do not include decomposition of gases flowing in the film. As shown in Figure 3c and the associated video, a periodic cycle of nucleation and detachment of bubbles appears to occur at the top of the tube, which is a characteristic feature of film boiling in general. The film boiling cycle has been described using Kelvin–Helmholtz instability theory as the mechanism for rising bubbles to coalesce, and the bubble spacing on the tube surface has been considered to correspond to a Taylor wavelength.<sup>27–33</sup>

As gases flow around the tube, they accumulate at the top and thicken the film; instabilities can develop, and bubbles will then depart from nodes with spacing corresponding to the Taylor wavelength  $\lambda = C \sqrt{\frac{\sigma}{g(\rho_L - \rho_g)}}$  where  $C = 2\pi\sqrt{3}$  for one-dimensional waves. For EtOH, Figure 3c shows four locations from which the four bubbles depart. The average bubble

spacing in Figure 3c is approximately 21 mm. Using saturated EtOH properties, the computed Taylor wavelength is  $\lambda \approx 17$  mm. The 14% difference with experiment is well within the –25 to +60% range noted in ref 28, which confirms the physics that govern the film boiling bubble departure cycle.

**3.2. Product Yield Rates.** There are two considerations for operation of a reactor based on film boiling. The first is that the reactor space must be created, which here is by formation of the vapor film (Figure 1). The second is that the temperature in the vapor film must be high enough for decomposition to occur at appreciable rates. When these conditions are met, decomposition will occur at measurable rates and be manifested by a product gas flow through the exhaust system that would not otherwise exist if decomposition did not occur (i.e., for the experimental design used here where the exhaust flow will contain only noncondensable gases).

Figure 4 shows the variation of noncondensable product gas volumetric flux with temperature.

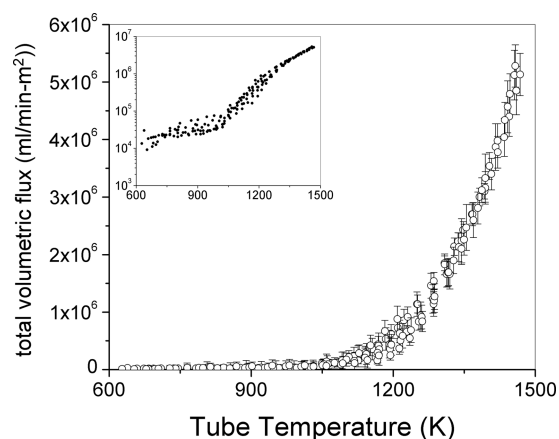


**Figure 4.** Total volumetric flux of exhaust gas flow rate from EtOH decomposition obtained from percolating bubbles. Inset expands scale of the same data (without uncertainty bars) to more clearly show fluxes over all temperatures.

The inset shows the same data on a logarithmic scale for greater clarity at low temperatures. The substantial increase of flow rate above 1000 K signals the emerging importance of EtOH decomposition from reactions initiated by C–C bond cleavage.

The individual species and their volumetric fluxes in the product gases were identified by GC analysis. As shown in Figure 5 six noncondensable stable species were detected in the gas product stream:  $H_2$ ,  $CO$ ,  $CH_4$ ,  $C_2H_4$ ,  $C_2H_6$ , and  $CO_2$ . Hydrogen has the highest concentration at all temperatures, which is consistent with theoretical predictions of EtOH decomposition that do not include inhibitors.<sup>3</sup>

Water is not among the gaseous species detected in the exhaust stream because it was condensed and refluxed to the liquid pool. It was not meaningful to compare the water concentration in the liquid with the concentrations of noncondensable stable gaseous products because the water concentration in the pool (shown in Table 1 for one particular condition) depends on the total liquid volume which is a control variable. More important is the relative concentration of species in the liquid (last column in Table 1). The acetaldehyde concentration is higher, which lends some support for a kinetic mechanism that includes decomposition of EtOH to

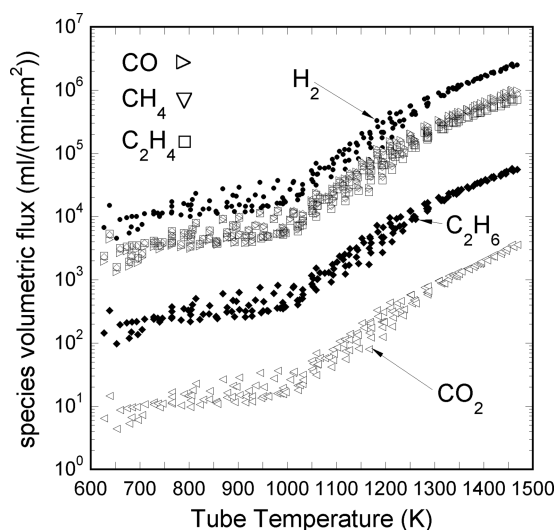


**Figure 5.** Volumetric flux of stable noncondensable products in exhaust stream from EtOH decomposition.

acetaldehyde, as noted below. Water is the third most abundant dissolved liquid, though its concentration is still small.

Figure 5 shows that below 1000 K the variation of volumetric fluxes with temperature is significantly weaker than at higher temperatures. Surface reactions of EtOH on an Inconel substrate have been reported with the importance of hydrogenation and dehydration reactions considered to form a carbon layer.<sup>24,25</sup> Surface reactions tend to have a lower activation energy compared to homogeneous reactions and, therefore, would result in a weaker dependence on temperature. This would be consistent with heterogeneous reactions being important at temperatures below around 1000 K in Figure 5 compared to higher temperatures. For surface reactions, the role of ethylene was speculated to be important in the process of forming carbon or coke through the transition that begins with ethylene.<sup>24</sup> It could proceed through acetylene,  $C_2H_4 \rightarrow$  acetylene  $\rightarrow$  polymers  $\rightarrow$  coke, where acetylene (though not detected) can be an unstable decomposition product of EtOH decomposition.

As seen in Figure 5, the order of concentrations in the product gas is approximately  $H_2 > [CO, CH_4, C_2H_4]$  (nearly the same)  $> C_2H_6 > CO_2$ . The hydrogen concentration in the exhaust gas is high in Figure 5 as contrasted to neat EtOH data reported in a flow reactor<sup>3</sup> (though the diagnostics used (i.e., an FTIR) would not be able to detect hydrogen). It is also interesting to note that simulations of a zero-dimensional reactor reported in ref 3 predict significant hydrogen formation without inhibitors present. Wall-catalyzed reactions are another source of hydrogen production from EtOH decomposition.<sup>24,25</sup>

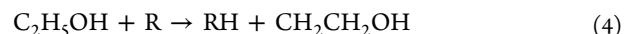
The species in Figure 5 would not all be present if eq 1 were the main EtOH decomposition route. For example, Park et al.<sup>1</sup> lists 10 reactions based on theoretical calculations in addition to eq 1 that involve H, OH, and  $CH_3$  radicals. Sivaramakrishana et al.<sup>20</sup> note 37 reactions for EtOH decomposition that involve intermediates. Here, C–C bond cleavage of EtOH to form radicals is an alternative route to initiate the EtOH decomposition process.

The chain branching route for EtOH decomposition includes the lowest energy channel<sup>20</sup> and begins with the formation of the methyl radical,

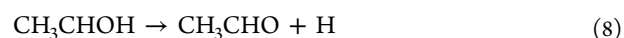


Numerous other radical reactions are also involved. A set of reactions is suggested to explain formation of stable products shown in Figure 5 that includes radical reactions as follows.

Radicals R (e.g.,  $R = CH_3, H, OH$ ) can attack EtOH via the reactions



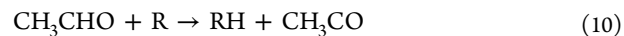
(if  $R = OH$  in any of the above, then water is formed). The products in eqs 3–5 can decompose to form additional radicals via the routes



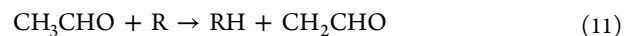
Decomposition of the  $CH_2OH$  radical from eq 2 gives formaldehyde and hydrogen as



Table 1 shows that acetaldehyde ( $CH_3CHO$ ) is the most prevalent condensable in the liquid pool. Its decomposition (which here would occur by preferentially vaporizing into the vapor film as noted previously) is well-characterized.<sup>34</sup> It can produce  $CH_3CO$  via the reaction



or  $CH_2CHO$  by the reaction



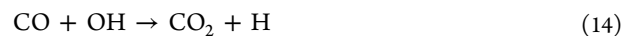
In eq 10, the radical abstracts a hydrogen atom from the acetyl group, while in eq 11, the radical abstracts a hydrogen atom from the methyl group of acetaldehyde to decompose acetaldehyde as,



Eq 12 is expected to be comparatively slow relative to eq 10 because the C–C bond energy is high in eq 12. The  $CH_3CO$  intermediate from eq 10 can decompose to produce CO by the reaction



And the CO can be attacked by OH

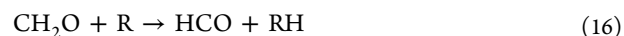


to provide a source of  $CO_2$  by conversion of CO in the system.

The  $CH_2CHO$  intermediate from eq 11 can decompose to form an H atom and ketene ( $CH_2CO$ ),



The formaldehyde from eq 9 can react with a radical to form HCO,



which in turn can decompose to form CO and H,

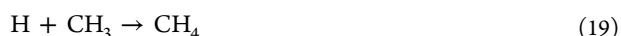


Eq 17 provides an alternative source of H and CO atoms.

To complete the overall sequence, H atoms may recombine to produce hydrogen



or react with methyl radicals to produce methane,



while ethane would form from



The multiple sources of H atoms in the above sequence are responsible for the abundance of hydrogen in the product stream (Figure 5) when no inhibitors are present.

The above sequence is based on the chain nature of EtOH decomposition without chemical inhibitors and explains the formation of the species in Figure 5. For every EtOH molecule decomposed by direct C–C bond cleavage (eq 2), many other EtOH decomposition reactions will occur to bring more radicals into the system. The reaction sequence also postulates the presence of a variety of stable species produced in the environment of film boiling. The decomposition process could be considerably simplified by removing intermediates through inhibitors that eliminate radical reactions and ostensibly leave eqs 1 and 2 as the sole means of decomposing EtOH. This remains a consideration for future studies in a film boiling reactor. As a final point, we are not able to determine rate parameters for individual reactions because a detailed numerical model for film boiling does not exist which includes decomposition in the vapor film.

#### 4. SUMMARY OF RESULTS

The results of the present study are summarized as follows. (1) The efficacy of film boiling to provide a thermal environment for decomposing EtOH was demonstrated. Overall, the products detected are consistent with prior work. (2) Film boiling of EtOH was maintained for tube surface temperatures between 627 and 1500 K (the highest value imposed in the experiments) at atmospheric pressure. At lower temperatures, the film destabilizes, and the reactor space disappeared. (3) In the absence of chemical inhibitors, H<sub>2</sub> had the highest concentration in the product stream, with lesser amounts of C<sub>2</sub>H<sub>4</sub>, CO, CH<sub>4</sub>, CO<sub>2</sub>, and C<sub>2</sub>H<sub>6</sub> detected. (4) Formation of the noncondensables is explained by a chain branching mechanism initiated by methyl radicals that provide additional routes to forming the stable species. (5) Evidence for heterogeneous reactions on the Inconel substrate is suggested below about 1000 K, where the variation of product yields with temperature was significantly lower than that at higher temperatures. (6) Several species were found in the liquid pool during prolonged operation that had transformed EtOH into a miscible mixture with acetaldehyde being in the largest concentration. The additional species detected in the liquid pool were a consequence of allowing condensable products to reflux to the chamber. (7) The morphology of film boiling consisted of bubble streams emanating from the top of the tube. The spacing of the streams was consistent with predictions from the Taylor wavelength of one-dimensional waves.

#### ■ ASSOCIATED CONTENT

##### ● Supporting Information

The Supporting Information is available free of charge on the ACS Publications website at DOI: 10.1021/acs.iecr.8b00770.

Video of transition from nucleate to film boiling of EtOH (ZIP)

#### ■ AUTHOR INFORMATION

##### Corresponding Author

\*E-mail: cta2@cornell.edu.

##### ORCID

C. Thomas Avedisian: 0000-0003-1343-584X

##### Present Addresses

□W.-C.K.: CGG, 10300 Town Park Drive, Houston, Texas 77072, United States.

○A.L.: Department of Mechanical Engineering, Virginia Polytechnic Institute and State University, Blacksburg, Virginia 24061, United States.

##### Notes

The authors declare no competing financial interest.

#### ■ ACKNOWLEDGMENTS

This project was supported in part by Grant 1336657 from the United States National Science Foundation with Dr. Jose L. Lage as the program manager. This support is greatly appreciated. Thanks are also due to Drs. Alfonso Ortega of Santa Clara University, Sumanta Acharya of the Illinois Institute of Technology, and Theodore Bergman of the University of Kansas for their interest in our work. The assistance with chemical analysis of liquid samples by GC/MS was provided by Dr. Xia Zeng of the Human Ecology Department at Cornell, and discussions with Dr. Ivan Keresztes of the Chemistry and Chemical Biology Department at Cornell are appreciated.

#### ■ ABBREVIATIONS

- A<sub>1</sub> = frequency factor for an Arrhenius rate expression
- E<sub>1</sub> = activation energy for eq 1<sup>1</sup>
- g = gravitational constant
- K<sub>1</sub> = Arrhenius rate constant for eq 1<sup>1</sup>
- R<sub>g</sub> = gas constant
- T = temperature
- σ = surface tension
- ρ<sub>L</sub> = liquid density
- ρ<sub>g</sub> = gas density

#### ■ REFERENCES

- (1) Park, J.; Zhu, R. S.; Lin, M. C. *Ab initio* molecular orbital/Rice–Ramsperger–Kassel–Marcus prediction of rate constant and product branching ratios. *J. Chem. Phys.* **2002**, *117*, 3224–3231.
- (2) Li, J.; Kazakov, A.; Dryer, F. L. Experimental and Numerical Studies of Ethanol Decomposition Reactions. *J. Phys. Chem. A* **2004**, *108*, 7671–7680.
- (3) Li, J.; Kazakov, A.; Dryer, F. L. Ethanol Pyrolysis Experiments in a Variable Pressure Flow Reactor. *Int. J. Chem. Kinet.* **2001**, *33*, 859–867.
- (4) Wu, C. W.; Matsui, H.; Wang, H. S.; Lin, M. C. Shock Tube Study on the Thermal Decomposition of Ethanol. *J. Phys. Chem. A* **2011**, *115*, 8086–8092.
- (5) Marinov, N. M. A Detailed Chemical Kinetic Model for High Temperature Ethanol Oxidation. *Int. J. Chem. Kinet.* **1999**, *31*, 183–220.
- (6) Haas, F. M.; Chaos, M.; Dryer, F. L. Low and intermediate temperature oxidation of ethanol and ethanol–PRF blends: An experimental and modeling study. *Combust. Flame* **2009**, *156*, 2346–2350.
- (7) Barraza-Botet, C. L.; Wagnon, S. W.; Wooldridge, M. S. Combustion Chemistry of Ethanol: Ignition and Speciation Studies in a Rapid Compression Facility. *J. Phys. Chem. A* **2016**, *120*, 7408–7418.

- (8) Cancino, L. R.; Fikri, M.; Oliveira, A. M.; Schulz, C. Measurement and Chemical Kinetics Modeling of Shock-Induced Ignition of Ethanol-Air Mixtures. *Energy Fuels* **2010**, *24*, 2830–21040.
- (9) Dagaut, P.; Boettner, J. C.; Cathonnet, M. Kinetic modeling of ethanol pyrolysis and combustion. *J. Chim. Phys. Phys.-Chim. Biol.* **1992**, *89*, 867–884.
- (10) Dong, L. Detailed influences of ethanol as fuel additive on combustion chemistry of premixed fuel-rich ethylene flames. *Sci. China: Technol. Sci.* **2015**, *58* (10), 1696–1704.
- (11) Frassoldati, A.; Cuoci, A.; Faravelli, T.; Ranzi, E. Kinetic Modeling of the Oxidation of Ethanol and Gasoline Surrogate Mixtures. *Combust. Sci. Technol.* **2010**, *182*, 653–667.
- (12) Glaude, P. A.; Fournet, R.; Bounaceur, R.; Molière, M. "Ethanol as an alternative fuel in gas turbines: Combustion and oxidation kinetics. Paper no. GT2010, Proc. ASME Turbo Expo 2010: Power for Land, Sea and Air; Glasgow, UK, June 14–18, 2010.
- (13) Kohse-Hoinghaus, K.; Oßwald, P.; Cool, T. A.; Kasper, T.; Hansen, N.; Qi, F.; Westbrook, C. K.; Westmoreland, P. R. Biofuel Combustion Chemistry: From Ethanol to Biodiesel. *Angew. Chem., Int. Ed.* **2010**, *49*, 3572–3597.
- (14) Olm, C.; Varga, T.; Valko, E.; Hartl, S.; Hasse, C.; Turanyi, T. Development of an Ethanol Combustion Mechanism Based on a Hierarchical Optimization Approach. *Int. J. Chem. Kinet.* **2016**, *48* (8), 423–441.
- (15) Sarathy, M.; Oßwald, P.; Hansen, M.; Kohse-Hoinghaus, K. Alcohol combustion chemistry. *Prog. Energy Combust. Sci.* **2014**, *44*, 40–102.
- (16) Vourliotakis, G.; Skevis, G.; Founti, M. A. Some aspects of combustion chemistry of C1–C2 oxygenated fuels in low pressure premixed flames. *Proc. Combust. Inst.* **2015**, *35*, 437–445.
- (17) Xu, H.; Yao, C.; Yuan, T.; Zhang, K.; Huijun, G. Measurements and modeling study of intermediates in ethanol and dimethyl ether low-pressure premixed flames using synchrotron photoionization. *Combust. Flame* **2011**, *158*, 1673–1681.
- (18) Vaidya, P. D.; Rodrigues, A. E. Insight into steam reforming of ethanol to produce hydrogen for fuel cells. *Chem. Eng. J.* **2006**, *117*, 39–49.
- (19) Morris, H. E. Reactions of Ethyl Alcohol. *Chem. Rev.* **1932**, *10*, 465–506.
- (20) Sivaramakrishnan, R.; Su, M. C.; Michael, J. V.; Klippenstein, S. J.; Harding, L. B.; Ruscic, B. Rate Constants for the Thermal Decomposition of Ethanol and Its Bimolecular Reactions with OH and D: Reflected Shock Tube and Theoretical Studies. *J. Phys. Chem. A* **2010**, *114*, 9425–9439.
- (21) Tsang, W. Energy Transfer Effects During the Multichannel Decomposition of Ethanol. *Int. J. Chem. Kinet.* **2004**, *36*, 456–465.
- (22) Szwarc, M. The Determination of Bond Dissociation Energies by Pyrolytic Methods. *Chem. Rev.* **1950**, *47*, 75–173.
- (23) Tsang, W.; Lifshitz, A. Shock Tube Techniques in Chemical Kinetics. *Annu. Rev. Phys. Chem.* **1990**, *41*, 559–599.
- (24) Amran, T.; Abdullah, T.; Croiset, E. Evaluation of an Inconel-625 Reactor and its Wall Effects on Ethanol Reforming in Supercritical Water. *Ind. Eng. Chem. Res.* **2014**, *53*, 2121–2129.
- (25) Arita, T.; Nakahara, K.; Nagami, K.; Kajimoto, O. Hydrogen Generation from Ethanol in Supercritical Water without Catalyst. *Tetrahedron Lett.* **2003**, *44*, 1083–1086.
- (26) Avedisian, C. T.; Kuo, W. C.; Tsang, W.; Lowery, A. High Temperature Thermal Decomposition of Diethyl Carbonate by Pool Film Boiling. *Ind. Eng. Chem. Res.* **2018**, *140* (6), 061501–1–061501–10.
- (27) Lienhard, J. H., IV; Lienhard, J. H., V. *A Heat Transfer Textbook*, 4th ed.; Phlogiston: Cambridge, MA, 2003; pp 476–490 (see also <http://ahtt.mit.edu>).
- (28) Son, G.; Dhir, V. K. Three-dimensional simulation of saturated film boiling on a horizontal cylinder. *Int. J. Heat Mass Transfer* **2008**, *51*, 1156–1167.
- (29) Son, G.; Dhir, V. K. Numerical Simulation of Saturated Film Boiling on a Horizontal Surface. *J. Heat Transfer* **1997**, *119*, 525–533.
- (30) Agarwal, D. K.; Welch, S. W. J.; Biswas, G.; Durst, F. Planar Simulation of Bubble Growth in Film Boiling in Near-Critical Water Using a Variant of the VOF Method. *J. Heat Transfer* **2004**, *126*, 329–338.
- (31) Esmaeeli, A.; Tryggvason, G. A front tracking method for computations of boiling in complex geometries. *Int. J. Multiphase Flow* **2004**, *30*, 1037–1050.
- (32) Carey, V. P. *Liquid-vapor phase change phenomena*; Taylor & Francis: United Kingdom, 1992; p 250.
- (33) Lienhard, J. H.; Wong, P. T. Y. The dominant unstable wavelength and minimum heat flux during film boiling on a horizontal cylinder. *J. Heat Transfer* **1964**, *86*, 220–225.
- (34) Gupte, K. S.; Kiefer, J. H.; Tranter, R. S.; Klippenstein, S. J.; Harding, L. B. Decomposition of Acetaldehyde: Experiment and Detailed Theory. *Proc. Combust. Inst.* **2007**, *31*, 167–174.